Applied Geochemistry 102 (2019) 108–120

Contents lists available at ScienceDirect

Applied Geochemistry

journal homepage: www.elsevier.com/locate/apgeochem

Tracking multiple Sr sources through variations in $^{87}Sr/^{86}Sr$ ratios of surface waters from the Aljustrel massive sulphide mining area: Geological *versus* anthropogenic inputs

A.T. Luís[a,b,*,1], N. Durães[a,1], E. Ferreira da Silva[a], S. Ribeiro[a], A.J.F. Silva[a], C. Patinha[a], S.F.P. Almeida[c], M.R. Azevedo[a]

[a] GeoBioTec – Department of Geosciences, University of Aveiro, Campus de Santiago, 3810-193 Aveiro, Portugal
[b] CESAM Associated Lab – Department of Biology, Campus de Santiago, 3810-193 Aveiro, Portugal
[c] GeoBioTec – Department of Biology, University of Aveiro, Campus de Santiago, 3810-193 Aveiro, Portugal

ARTICLE INFO

Editorial handling by Philippe Negrel

Keywords:
Aljustrel mine
$^{87}Sr/^{86}Sr$ ratios
Surface waters
Acid mine drainage
Chlorinated waters

ABSTRACT

This study presents major and trace element data and $^{87}Sr/^{86}Sr$ ratios for surface waters from a small watershed draining the Aljustrel sulphide mining area (South Portugal). The watershed is located in a geologically complex area comprising two main compartments: the northern compartment is dominated by Cenozoic formations and does not bear any mining activity, whilst the southern compartment is underlain by rocks from both the Cenozoic sedimentary cover and the mineralized sequences of the Variscan Paleozoic basement of the South Portuguese Zone.

Based on the available geochemical and isotopic data, the analysed water samples can be roughly divided into five main groups: (a) group 1 corresponds to AMD-contaminated water drainages from the southern part of the catchment, showing pH < 4.0, high dissolved sulphate and heavy metal/metalloid contents and $^{87}Sr/^{86}Sr$ ratios ranging from 0.7101 to 0.7126; (b) group 2 is represented by unpolluted stream waters from the northern compartment, having pH > 8, marked depletions in SO_4 and heavy metals and displaying Sr isotopic compositions similar to rainwater ($^{87}Sr/^{86}Sr$ = 0.7097–0.7098); (c) group 3 includes mixed-type stream waters with pH and elemental/isotopic signatures intermediate between those of groups 1 and 2; (d) group 4 comprises the samples collected at two lime-treated water dams from the mining area, that are clearly distinguished from the impacted waters of group 1 by their elevated Ca, Mg and Sr concentrations and low $^{87}Sr/^{86}Sr$ ratios ($^{87}Sr/^{86}Sr$ = 0.7085–0.7091); (e) group 5 includes clean waters from two dams located upstream of the ore processing site, which are dominantly supplied by direct precipitation and surface runoff and have pH > 6, very low SO_4 and metal concentrations and $^{87}Sr/^{86}Sr$ ratios varying between 0.7094 and 0.7108.

Variations in the $^{87}Sr/^{86}Sr$ ratios and Sr concentrations of the analysed waters are attributed to mixing of two main end-members: atmospheric meteoric waters (local rainfall/runoff) with low Sr contents and $^{87}Sr/^{86}Sr$ ratios ≈ 0.7095 and more radiogenic waters derived from the Aljustrel mining area. The highly radiogenic signatures of the southern tributaries appear to have been controlled by weathering of plagioclase from the acid volcanic rocks of the Paleozoic basement, enhanced by mining activities (pyrite oxidation), although released strontium from gangue carbonates could have locally contributed to the fluctuations of Sr contents and $^{87}Sr/^{86}Sr$ ratios observed in some of these water samples. By contrast, the low $^{87}Sr/^{86}Sr$ ratios and relatively high Sr (Cl and Na) concentrations shown by the surface waters draining the northern compartment suggest that these tributaries correspond to meteoric waters that have gained Cl, Na and Sr through wash-out of Cenozoic deposits containing finely disseminated halite layers. Finally, the decrease in the $^{87}Sr/^{86}Sr$ ratios and elevation of Sr contents observed in the samples from the lime-treated water dams support the involvement of an anthropogenic source of Sr with $^{87}Sr/^{86}Sr$ ratios lower than that of rainfall.

* Corresponding author. GeoBioTec – Department of Geosciences, University of Aveiro, Campus de Santiago, 3810-193 Aveiro, Portugal.
E-mail address: anatluis@ua.pt (A.T. Luís).
[1] The two authors contributed equally to the manuscript elaboration.

https://doi.org/10.1016/j.apgeochem.2019.01.016
Received 30 May 2018; Received in revised form 27 December 2018; Accepted 28 January 2019
Available online 30 January 2019
0883-2927/

1. Introduction

Strontium isotopes are powerful geochemical tracers and have increasingly been applied to a broad range of hydrologic systems for constraining water sources and water mixing processes (e.g. Åberg, 1995; Capo et al., 1998; Semhi et al., 2000; Frost et al., 2002; Frost and Toner, 2004; Négrel and Pauwels, 2004; Négrel et al., 2007; Brenot et al., 2008; Tichomirowa et al., 2010; Peiffer et al., 2011; Zieliński et al., 2016) and/or assessing water–rock interactions, flow paths and weathering rates (e.g. Palmer and Edmond, 1992; Bullen et al., 1996; McNutt, 2000; Shand et al., 2009; Bataille and Bowen, 2012; Brennan et al., 2014).

A wide number of studies have shown that strontium isotopes can also be used to monitor contamination of natural water systems by anthropogenic inputs, such as fertilizers, waters from mine drainage, industrial waste waters, hydraulic fracturing fluids and urban pollutants (e.g. Böhlke and Horan, 2000; Hosono et al., 2007; Jeon, 2008; Pierson-Wickmann et al., 2009; Hosono et al., 2010; Chapman et al., 2013; Vengosh et al., 2013; Shin et al., 2015).

More recently, the range of applications of Sr isotopes was expanded to new research areas, including forensics (e.g. Beard and Johnson, 2000), archaeology (e.g. Hodell et al., 2004; Bentley et al., 2008), ecology (e.g. Koch et al., 1995; Chamberlain et al., 1997; Hoppe et al., 1999) and food and beverage industry (e.g. Kelly et al., 2005; Montgomery et al., 2006; Voerkelius et al., 2010).

In the particular case of surface waters affected by metal-rich drainage from mining activities, Sr isotopes have proven to be of limited use for distinguishing contaminated from uncontaminated stream waters, but provide crucial information on variations in the bedrock geology, water-rock interactions, chemical weathering processes and relative contribution of natural and anthropogenic Sr sources with contrasting isotopic compositions (e.g. Jeon, 2008; Deng et al., 2009; Christian et al., 2011; Vengosh et al., 2013; Khaska et al., 2015).

This study presents Sr isotopic data for discharge effluents from the Aljustrel sulphide mine and stream waters draining the area with the aim of better understanding the potential sources of lithologic and anthropogenic Sr in the region and the effects of mixing of surface waters originating from those sources. The results obtained are expected to improve our knowledge on the factors controlling surface-water chemistry in this mineralized area and guide future investigations of background water quality in geologically complex watersheds affected by historical mining activity.

2. Strontium isotopes in surface waters

Strontium is a divalent alkaline earth element with four stable naturally-occurring isotopes (^{84}Sr, ^{86}Sr, ^{87}Sr, ^{88}Sr). Of these, ^{87}Sr is radiogenic and forms by the radioactive decay of ^{87}Rb (with a half-life of 48 billion years). As a result, the amount of the daughter (radiogenic) isotope in rocks and minerals increases with geological age whilst the abundance of the parent (radioactive) isotope decreases over time (Faure, 1986; Faure and Mensing, 2005).

Strontium (Sr^{2+}) can easily substitute Ca^{2+} in the crystal lattice of Ca-bearing minerals, such as plagioclase, apatite, gypsum, calcite, aragonite and dolomite, while rubidium (Rb^{+}) is incorporated in K-bearing silicate minerals, including K-feldspars, micas and clay minerals (Faure, 1986; Faure and Mensing, 2005). Therefore, old sialic crustal rocks containing minerals with high Rb/Sr ratios tend to show highly radiogenic Sr isotopic signatures ($^{87}Sr/^{86}Sr$ ratios > 0.709), young basaltic rocks depleted in Rb are characterized by low to very low $^{87}Sr/^{86}Sr$ ratios (0.703–0.706) and Sr-enriched calcareous sediments and limestones have, in general, intermediate $^{87}Sr/^{86}Sr$ ratios (between 0.706 and 0.709) (e.g. Faure, 1986; Faure and Mensing, 2005; McNutt, 2000; Shand et al., 2009).

Unlike H, C, N and O, Sr isotopes are not significantly affected by mass fractionation during chemical weathering processes and can thus be transferred from bedrock to natural waters, soils, interstitial soil waters, biosphere and food chains without appreciable changes of the $^{87}Sr/^{86}Sr$ ratios (e.g. Capo et al., 1998; Shand et al., 2009; Frei and Frei, 2011).

Although the Sr isotopic composition of surface and groundwater reflects, to a large extent, the nature of the local bedrock undergoing alteration, the degree to which Sr is released to the water is strongly dependent on the reaction kinetics of mineral dissolution. As shown by Åberg et al. (1989), minerals with different Rb/Sr ratios and $^{87}Sr/^{86}Sr$ ratios weather at different rates leading, in many cases, to a pronounced decoupling between the solute Sr isotope ratios and those of the parent rock (e.g. Åberg et al., 1989; Blum et al., 1993; Bullen et al., 1996; Shand et al., 2009).

Atmospheric inputs, residence time and anthropogenic disturbances are other factors that may greatly influence the Sr isotopic ratios of freshwater systems. Hence, the application of Sr isotopes as tracers of surface water origin, mixing relationships and hypothetical end-member components requires a thorough isotopic characterization of all possible sources of Sr (bedrock geology and age, "weathering-derived" Sr, rainfall, anthropogenic contaminants) in conjunction with a sound knowledge of the processes taking place along flow pathways (Capo et al., 1998; Shand et al., 2009).

3. Study area

The Aljustrel mine is located in the northwestern sector of the so-called Iberian Pyrite Belt (IPB), one of the largest provinces of volcanogenic massive sulphide ore deposits in the world (e.g. Barriga, 1990; Leistel et al., 1998; Carvalho et al., 1999; Sáez et al., 1999; Tornos, 2006). With a total area of approximately 250 km by up to 60 km, the IPB is part of the Variscan basement of Iberia and constitutes one of the main tectonostratigraphic domains of the South Portuguese Zone (SPZ) (Fig. 1; Oliveira, 1990; Silva et al., 1990).

The stratigraphic record of the IPB comprises three main units: (a) the Late Devonian Phyllite–Quartzite Group (PQ), (b) the Famennian to mid-late Visean Volcano-Sedimentary Complex (VSC) and (c) the late Visean to mid-late Pennsylvanian Culm Group (Schermerhorn, 1971) (Fig. 1). Lying at the base of the sequence, the PQ Group consists of shales and quartz-rich sandstones deposited in a shallow marine shelf environment (Schermerhorn, 1971; Oliveira, 1990; Silva et al., 1990). The VSC is composed of submarine felsic volcanic, subvolcanic and volcanoclastic rocks and minor mafic occurrences (basalts and dolerites), interbedded with shales and siltstones (e.g. Oliveira, 1990; Silva et al., 1990; Inverno et al., 2015). Most of the IPB massive sulphide ore deposits and related hydrothermal mineralized stockworks are hosted in the VSC and tend to occur either on the top of the felsic volcanic sequences or in close association with black shales (e.g. Barriga, 1990; Mitjavila et al., 1997; Thiéblemont et al., 1998; Relvas et al., 2001, 2006a; 2006b; Oliveira et al., 2013; Tornos, 2006; Rosa et al., 2010; Inverno et al., 2015; Martin-Izard et al., 2016). Finally, the Culm Group is dominated by a flyshoid sequence of synorogenic turbidites (shales, sandstones and rare conglomerates) (e.g. https://www.sciencedirect.com/science/article/pii/S0169136816300658, Oliveira, 1990).

The whole IPB series was affected by deformation and low-grade regional metamorphism during the Variscan Orogeny (Munhá, 1990). Major Variscan structures within the IPB include south-verging folds, axial plane slaty cleavages and thrusts with strikes varying from NW-SE in the west-central part of the IPB to W-E in the eastern sector (Fig. 1; Oliveira, 1990; Silva et al., 1990). The last Variscan tectonic imprint on the IPB is related to the development of two sets of conjugate strike-slip fault systems: a set of dominant NNW-SSE striking dextral faults and a set of NE-SW to ENE-WSW striking sinistral faults.

As shown in the more detailed geological map of Fig. 2, the studied area lies in the contact between the deformed VSC and Culm sequences of the Paleozoic basement of the SPZ and the Cenozoic cover deposits of the Sado Basin. The boundary is marked by a major fault (the sinistral

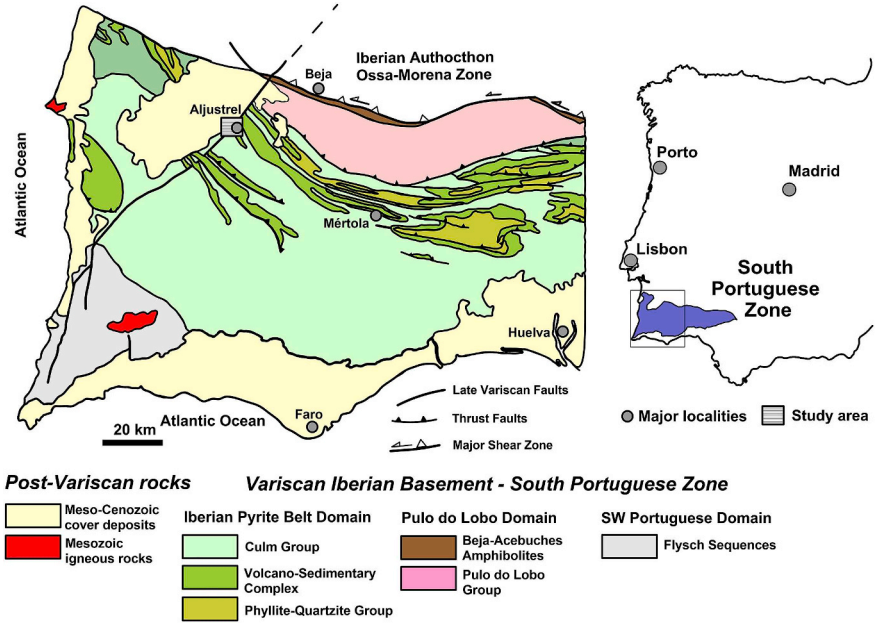

Fig. 1. Simplified geological map showing the main tectonostratigraphic domains of the South Portuguese Zone (SPZ) and the location of the Aljustrel mining area (modified from Oliveira, 1990 and Silva et al., 1990).

NE-SW trending Messejana fault), which was reactivated during the Cenozoic leading to the downward movement of the NW block. From Paleogene to Neogene and Quaternary times, the fault-bounded subsident block was infilled with fluvial and marine sediments originating the so-called Sado Basin (Pimentel, 1998, Pais et al., 2012 and references therein). In the Aljustrel region, the Cenozoic sedimentary rocks cover extensive areas and include late Paleogene alluvial-fans (coarse conglomerates and sandstones, interlayered with lutites from the Vale do Guizo Formation), late Miocene sandy-clay fluvio-marine deposits (Esbarrandadoiro Formation), Pliocene fluvial sands/alluvial-fans and Quaternary unconsolidated alluvial deposits (Fig. 2; Schermerhorn et al., 1987; Pimentel, 1998).

Occupying the southeastern sector of the studied area, the Aljustrel mining district consists of six main orebodies (S. João, Moinho, Algares, Estação, Feitais and Gavião) hosted in shales and acid volcanic rocks from the VSC (Fig. 2). The sulphide mineral assemblages of these orebodies contain mostly pyrite and minor amounts of sphalerite, chalcopyrite, arsenopyrite, tetrahedrite, galena, kobellite-tintinaite,

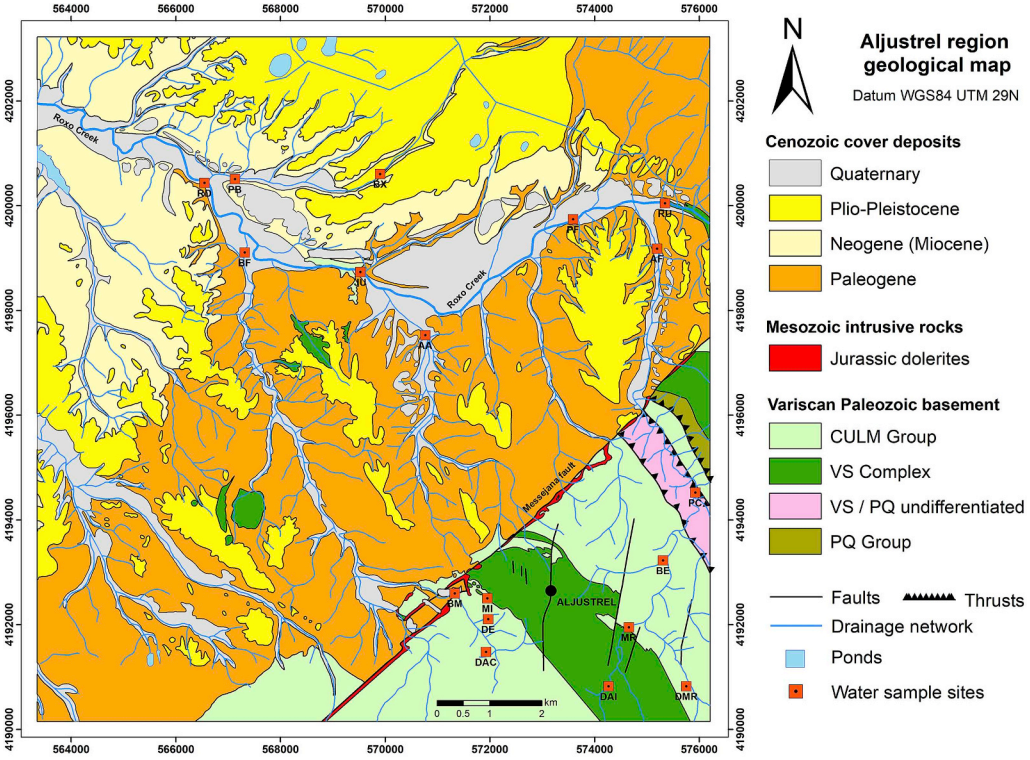

Fig. 2. Geological map of the Aljustrel area (simplified from Schermerhorn et al., 1987). Red symbols stand for water sampling sites. (For interpretation of the references to colour in this figure legend, the reader is referred to the Web version of this article.)

stannite, pyrrhotite and bismuth (Barriga and Fyfe, 1998; Sáez et al., 1999; Relvas et al., 2011). The origin of the IPB polymetallic sulphide deposits and the relationships between ore formation, magmatism and tectonics have been addressed by a large number of authors (e.g. Barriga, 1990; Mitjavila et al., 1997; Thiéblemont et al., 1998; Relvas et al., 2001, 2006a; 2006b; Oliveira et al., 2013; Tornos, 2006; Rosa et al., 2010; Martin-Izard et al., 2016).

Mining activity at Aljustrel began at the end of the 3rd millennium BC, continued during Roman times and, after several centuries of inactivity, pyrite recovery for copper and acid sulphuric production gained a strong increment in the XIX and XX centuries (Nocete et al., 2005; Tornos, 2006). Following several periods of closure, the mine reopened in 2008 and is presently being exploited for Zn and Cu.

Mechanical and chemical weathering of exposed massive sulphides, waste rock dumps and tailing dams caused long-lasting environment impacts in the area. In particular, acid mine drainage (AMD) resulting from the oxidation of sulphur and As-bearing minerals by runoff waters and infiltrated rainwater promoted the release of significant amounts of As and metals into stream waters, groundwater, soils, vegetation and sediments (e.g. Luís et al., 2009, 2016; Candeias et al., 2011). From 2006 to 2015, a large campaign of decontamination, confining and rehabilitation was carried out by EDM (a public capital company) on old mining sites from the Aljustrel area (Carvalho et al., 2016). Nevertheless, As and metal contamination of stream waters still persists.

Overall, the studied area is dominated by dry Mediterranean almost semi-arid conditions with a mean annual temperature of 20 °C and high evapotranspiration rates (Chambel and Almeida, 2000). Long-term mean annual rainfall in the catchment area is estimated in the range of 500–550 mm (Yevenes and Mannaerts, 2012).

The present investigation was focused on the Ribeira do Roxo watershed, a small water catchment within the Aljustrel region (Fig. 2). The Roxo creek flows westwards through the Cenozoic sedimentary deposits of the Sado Basin receiving perennial drainages from the northern and southern slopes. While the northern part of the watershed is dominated by Cenozoic formations and does not bear any mining activity, the southern compartment is underlain by rocks from both the Cenozoic sedimentary cover and the mineralized sequences of the Paleozoic basement of the SPZ (Fig. 2). Therefore, the tributaries crossing active and reclaimed sections of the Aljustrel mining area are all potentially contaminated.

4. Methods

4.1. Sampling and field measurements

Surface water samples were collected from 13 streams, 4 water dams and 1 discharge effluent from the Aljustrel sulphide mine during four sampling campaigns in two hydrological years. Of the 13 stream water samples, 4 were collected from tributaries of the Roxo creek receiving direct discharges from the Aljustrel mining area, 2 from tributaries running through Cenozoic rocks of the northern compartment unaffected by mining activity and the remaining samples from sites located either along the main stem of the Roxo creek or close to the confluence of minor streams with the main creek (Fig. 2; Table 1). Two of the four sampled water dams collect AMD and use lime treatment to increase pH and reduce metal (loid) contents (DAC and DE), whilst the other two are located upstream from the ore processing site (DAI and DMR) (Fig. 2; Table 1). An additional sample of rainwater was also collected for comparison.

All water samples were collected in 1L acid-washed polyethylene bottles, transferred in cool boxes to the laboratory where they were filtered through a 0.45 µm Millipore membrane filter using a vacuum pumping system and then stored at 4 °C in the dark until analysis. Filtered water samples were divided into three aliquots: one aliquot was stored without acidification for anion analysis, whereas the other two for major cation, dissolved metal (loid)s and Sr isotope analysis were acidified with 1 mL of ultra-pure HNO_3 to a pH of ~2.

The field parameters (temperature, pH and electrical conductivity) were measured in the field using a multiprobe WTW Multiline P4 SET previously calibrated with standard buffer solutions covering the observed range of pH and EC values. Alkalinity (as HCO_3) was determined on site by acidic titration with 0.16N H_2SO_4.

4.2. Elemental analyses

Major cation, dissolved metal (loid)s and Sr concentrations were determined by inductively coupled plasma mass spectrometry (ICP-MS) at ACME Analytical Laboratories Ltd., Canada (ACME Anal. ISO 9002 Accredited Lab, Canada). Sulphate was measured by ion chromatography at the Laboratory of Geochemistry of the Department of Geosciences of the University of Aveiro. Precision and bias, assessed by replicate analyses of certified reference materials (STANDARD WASTWATRA6), blanks and unknown samples, were less 10% for sulphate, cations, trace metal (loid)s and strontium. A full description of the water samples analysed in the present study is given by Luís et al. (2009, 2016), including their collection, handling, preparation protocols and main geochemical characteristics.

4.3. Sr isotope analysis

Strontium isotopic ratios were determined by thermal ionisation mass spectrometry (TIMS) on a multi-collector VG-Sector 54 mass spectrometer at the Laboratory of Isotope Geology of the University of Aveiro using a dynamic measurement mode. In the laboratory, the water samples were first pipetted into Savillex Teflon beakers and dried down. The residue was subsequently acidified with 1 mL sub-boiled 23 M HF and 0.5 mL sub-boiled 14 M HNO_3, dried and redissolved in 6 M HCl. Strontium separation followed a conventional ion-exchange chromatography procedure, using quartz columns filled with Bio-Rad® AG50W X8 (200–400 mesh) resin and 2.5 M HCl as eluent. After evaporation, Sr samples were loaded onto central tantalum filaments with 1 M H_3PO_4 and analysed by TIMS. All measured $^{87}Sr/^{86}Sr$ ratios were corrected for instrumental mass fractionation using $^{86}Sr/^{88}Sr = 0.1194$. Reproducibility and accuracy of Sr isotope runs have been periodically checked by running the Standard Reference Material SRM 987, with a mean $^{87}Sr/^{86}Sr$ value over the period of analysis of 0.710263 ± 6 (n = 24, confidence limit = 95%). Analytical blanks were negligible (less than 0.2 ng).

5. Results

5.1. Hydrochemical data

Overall, the analysed water samples show a wide spectrum of pH values (pH = 2.0–8.7) and electrical conductivity (EC) ranging from 114 to 14,200 µS cm^{-1} (Luís et al., 2009, 2016). The type and abundance of major anions and cations in the studied waters and their trace element signatures are also variable (Table 2; Luís et al., 2009, 2016). Using pH as a discrimination index, the water samples from the Aljustrel region can be roughly divided into five main groups (Table 2; Figs. 2 and 3): (a) group 1 corresponds to AMD-contaminated water drainages from the mining area (MI, MR, BE, PC, AF); (b) group 2 comprises the AMD-uncontaminated stream water samples flowing through the northern branch of the Roxo creek watershed (PB and BX); (c) group 3 includes mixed-type water samples with pH and elemental compositions intermediate between those of groups 1 and 2 (RU, PF, AA, JU, BF, RD); (d) group 4 is represented by the samples collected in two lime-treated water dams (DAC, DE) from the mining area and one tributary fed by the DE dam (BM) and (e) group 5 includes the water samples from two dams located upstream of the ore processing site (DAI and DMR).

Table 1
– Sample location, water type and bedrock geology of surficial water samples from the Aljustrel region.

Sample ID	Site name	Sample location	Water type	Bedrock geology
MI	Aljustrel mine	Aljustrel mine	AMD-contaminated	Paleozoic metamorphic basement
MR	Monte Ruas	Roxo creek tributary	AMD-contaminated	Paleozoic metamorphic basement
BE	Porto Beja	Roxo creek tributary	AMD-contaminated	Paleozoic metamorphic basement
PC	Ponte Curval	Roxo creek tributary	AMD-contaminated	Paleozoic metamorphic basement
AF	Água Forte	Roxo creek tributary	Mixed -type	Cenozoic deposits from southern slope
AA	Água Azeda	Roxo creek tributary	Mixed -type	Cenozoic deposits from southern slope
BF	Barranco Farrobo	Roxo creek tributary	Mixed -type	Cenozoic deposits from southern slope
RU	Roxo	Roxo creek main stem	Mixed -type	Cenozoic deposits
PF	Porto Ferreira	Roxo creek main stem	Mixed -type	Cenozoic deposits
JU	Jungeiros	Roxo creek main stem	Mixed -type	Cenozoic deposits
RD	Roxo Jusante	Roxo creek main stem	Mixed -type	Cenozoic deposits
PB	Pero Bonito	Roxo creek tributary	AMD-uncontaminated	Cenozoic deposits from northern slope
BX	Barranco Xacafre	Roxo creek tributary	AMD-uncontaminated	Cenozoic deposits from northern slope
DAI	Águas Industriais	Water dam	AMD-uncontaminated	Paleozoic metamorphic basement
DMR	Monte Ruas	Water dam	AMD-uncontaminated	Paleozoic metamorphic basement
DAC	Águas Claras	Water dam	Lime treated	Paleozoic metamorphic basement
DE	Estéreis	Water dam	Lime treated	Paleozoic metamorphic basement
BM	Barranco Morgado	Stream sourced by DE	Lime treated	Paleozoic metamorphic basement

In spite of some scatter, the samples from groups 1, 2 and 3 tend to define broad coherent trends on most chemical variation diagrams of Fig. 3. The AMD-contaminated water samples (group 1) show the lowest pH (pH < 4,0) and the highest dissolved sulphate (SO_4 > 850 mg L^{-1}), heavy metal/metalloid (Cu, Zn, Pb, Mn, Cd, Fe, As) and Al contents, whilst the AMD-uncontaminated stream waters (group 2) plot at the extreme alkaline end of the observed trends (pH > 8) and exhibit a clear enrichment in Cl and Na (Cl > 592 mg L^{-1}; Na > 200 mg L^{-1}), accompanied by a strong depletion in SO_4, heavy metals/metalloids and Al (Fig. 3; Table 2). Lying between the samples from groups 1 and 2, the stream waters of group 3 display a complex compositional pattern that appears to reflect the influence of variable inputs from two distinct sources (contaminated and uncontaminated waters) (Fig. 3; Table 2). Note that all the mixed water samples were collected either down-gradient drainages coming from the mining area (southern compartment) or at the confluence between these drainages and the main Roxo creek (Fig. 2).

As a result of lime addition, the AMD-contaminated dam waters from sites DAC and DE and the effluent BM (group 4) can be clearly distinguished from the mining impacted samples of group 1 by their elevated Ca, Mg and Sr concentrations, but still exhibit pH values and levels of SO_4 and dissolved metals similar to group 1 samples (Fig. 3; Table 2). In contrast, the waters stored at the DAI and DMR dams (both located upstream from the ore processing site) are dominantly supplied by direct precipitation and surface runoff and have pH ranging from 6.3 to 8.7 and very low SO_4 and metal (loid) concentrations (Fig. 3; Table 2).

Table 2
Physicochemical parameters (pH, EC) and range of major and trace element concentrations for the main groups of water samples.

Parameter	Rainwater	Mine Water	AMD-contaminated streams *Group 1*	Mixed-type waters *Group 3*	AMD-uncontaminated streams *Group 2*	AMD-uncontaminated water dams *Group 5*	Lime treated water dams *Group 4*
		Min-Max					
pH	≈7	2.9–4.1	2.0–2.7	3.4–8.4	8.0–8.4	6.3–8.7	2.4–8.1
EC (µs cm^{-1})	45	8000 - 8350	1689 - 14200	1451 - 3500	390 - 3690	458 - 1114	3400–7900
HCO_3^- (mg L^{-1})	6.3	0	0	0–986	247–917	67–385	0–276
SO_4^{2-} (mg L^{-1})	3	7257 - 8584	858–22601	23 - 2179	83–292	32–93	2196–5660
Cl^- (mg L^{-1})	9	122–188	22–307	258–760	592 - 1049	67–151	131–199
Ca (mg L^{-1})	8	429–573	61–424	98–388	155–231	32–45	575–828
Na (mg L^{-1})	6.1	159–206	17–177	158–317	201–337	52–83	167–296
K (mg L^{-1})	2.1	5.9–6.4	0.3–11	1.0–6.9	0.9–2.2	3.9–7.1	11–29
Mg (mg L^{-1})	2.1	665 - 1396	42–668	65–196	113–167	17–157	241–854
Fe (mg L^{-1})	0.03	383–836	21 - 6157	0.01–0.64	0.01–0.03	0.01–0.10	0.05–163
Al (mg L^{-1})	0.02	115–208	26 - 1455	0.001–20	0.001–0.016	0.002–0.019	0.2–34
Si (µg L^{-1})	59	13276–38040	6479 - 59317	3499 - 15736	7559 - 10697	348 - 2756	1559–11951
Cu (µg L^{-1})	8.5	16258–23522	5541 - 264869	1 - 5076	1.3–4.4	2.2–15	61–7951
Zn (µg L^{-1})	164	429844–549927	23663–970418	0.3–20159	0.7–8.5	1.4–67	497–497493
Mn (µg L^{-1})	7.8	130042–222943	4179 - 116575	0.03 - 7698	0.03–79	0.03–660	584–141584
As (µg L^{-1})	0.25	25–132	3–29891	1.7–9.5	5–10	2.4–5.9	5.6–960
Rb (µg L^{-1})	4.6	26–94	0.4–22	0.7–6.9	0.7–1.0	1.2–2.3	17–57
Sr (µg L^{-1})	28	1419 - 1633	40–506	362–872	759 - 1305	144–234	549–834

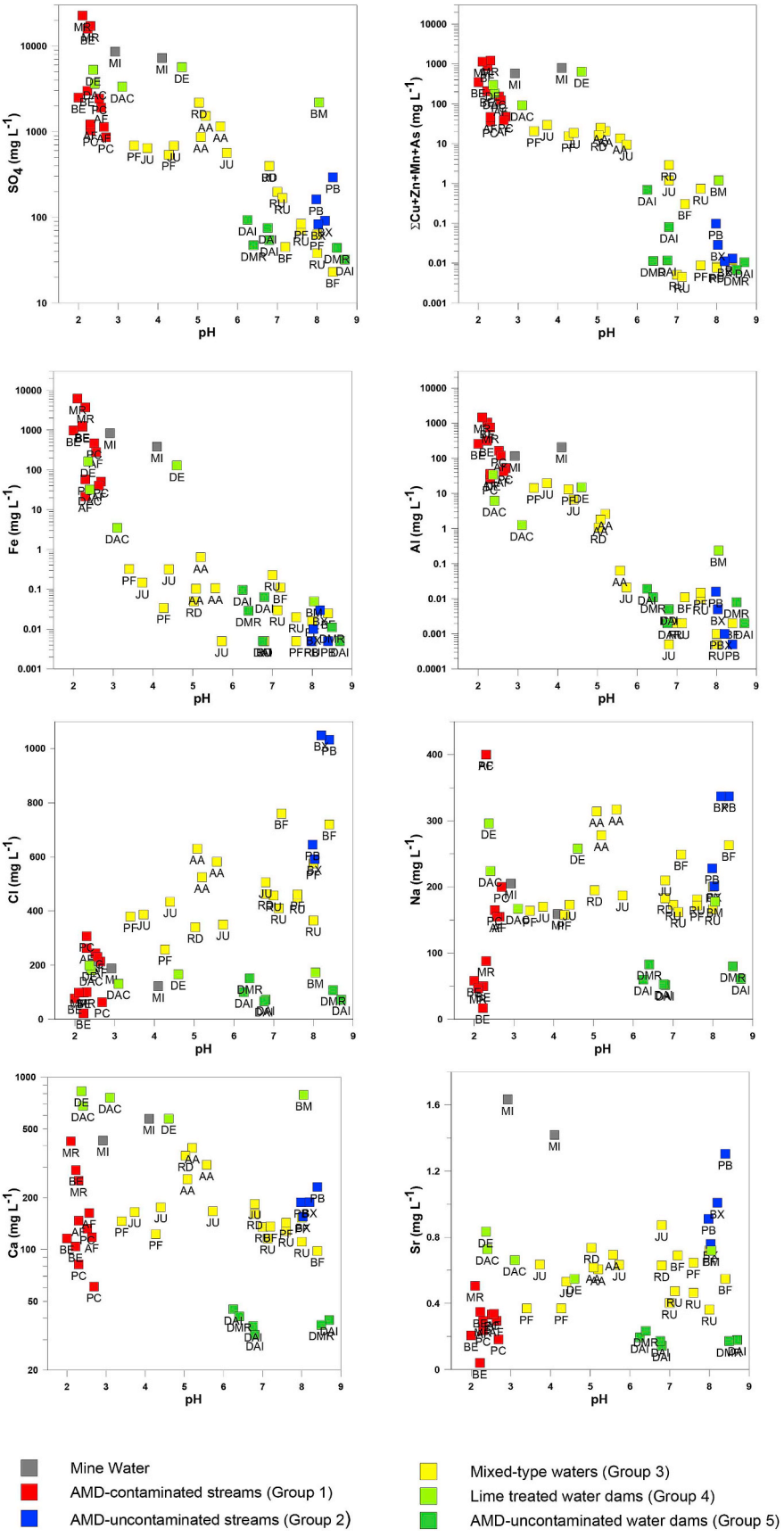

Fig. 3. Chemical variation diagrams as a function of pH for the surface waters from the Roxo Creek watershed.

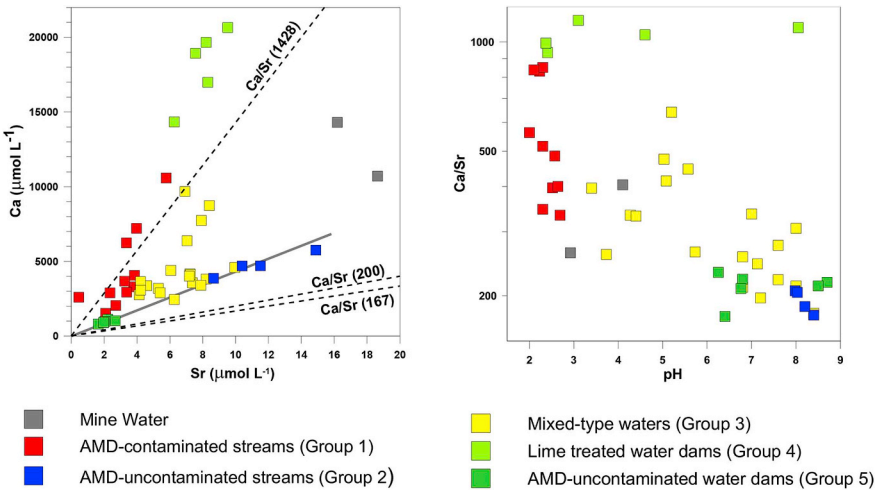

Fig. 4. (a) Relationship between Ca and Sr concentrations (in µmol L^{-1}) for the surface waters from the Roxo Creek watershed; (b) Variation of Ca/Sr ratios as a function of pH in the analysed waters. Dotted lines indicate Ca/Sr ratios of monolithic catchments reported by Meybeck (1986): mafic silicates Ca/Sr = 167 µmol/µmol, felsic silicates Ca/Sr = 200 µmol/µmol and pure carbonates Ca/Sr = 1428 µmol/µmol.

With the exception of the clean waters from the DAI and DMR reservoirs (group 5), which display the lowest Ca and Sr contents and plot as a discrete cluster of data points in the diagrams Ca *vs* pH and Sr *vs* pH (Fig. 3), there is no distinct correlation between Ca and pH and Sr and pH for most of the remaining water samples (Fig. 3). Strontium concentrations range from 50 to 406 µg L^{-1} in the AMD-contaminated waters (group 1), increase to values of 759–1305 µg L^{-1} in the unpolluted stream waters from group 3, but do not show a regular variation within the samples of group 2. Calcium behaviour is even more scattered (Ca = 32–421 mg L^{-1}; Fig. 3).

It is worth noting that the waters collected at site MI (mine water) are enriched in Ca and Sr compared to all the other samples (Fig. 3; Table 2), suggesting that they may correspond to groundwater discharges that have interacted with Ca− and Sr-bearing minerals at deeper levels. The occurrence of carbonate gangue minerals associated with the massive ore deposits of the Aljustrel mining area has been reported by several authors (Barriga and Carvalho, 1983; Gaspar, 1996; Inverno et al., 2008) and could have contributed to increase the amounts of dissolved Ca and Sr in these waters.

When plotted on the Ca *vs.* Sr and Ca/Sr *vs.* pH diagrams (Fig. 4), the samples from group 1 display higher Ca contents (though widely variable), higher Ca/Sr ratios and lower Sr concentrations than those of group 2, whereas the waters from group 3 have transitional geochemical signatures between the samples of groups 1 and 2. Consistent with the fact that all the sampled stream waters drain bedrock lithologies dominantly composed by silicates, most of the analysed waters define a trend located just above the Ca/Sr lines observed in mixed silicate catchments (Ca/Sr = 167–200, Meybeck, 1986). As there are no carbonate outcrops in the studied area, the shift of some points towards the "carbonate line" (Meybeck, 1986) can be attributed to local Ca inputs from another source, possibly related to residues of ore processing.

During the monitoring period, significant fluctuations in pH and chemical composition were observed within the water samples collected at the same site (Fig. 3). This may reflect mixing of water inflows from several sources and/or variations in the dissolution rates of primary and secondary minerals in response to changes in the hydrological conditions (low/high flow cycles).

5.2. $^{87}Sr/^{86}Sr$ isotope ratios

As illustrated in Fig. 5 and Table 3, the $^{87}Sr/^{86}Sr$ ratios of the studied water samples are highly scattered, ranging from 0.708530 to 0.712694. The waters from the DAC and DE lime-treated dams (group 4) have the lowest $^{87}Sr/^{86}Sr$ ratios ($^{87}Sr/^{86}Sr$ = 0.70853–0.70919) and exhibit Sr isotopic compositions less radiogenic than that of the single rainfall sample collected in this study ($^{87}Sr/^{86}Sr$ = 0.709460 ± 33; Fig. 5; Table 3), supporting the involvement of an anthropogenic source of Sr with low $^{87}Sr/^{86}Sr$ ratios (CaO lime) to these waters (Christian et al., 2011; Khaska et al., 2015; Harkness et al., 2016).

On the other hand, both the unpolluted stream waters that flow through the alluvial and fluvial Cenozoic sediments (group 2) and the clean waters stored at the DAI waterproofing dam (group 5) show Sr isotopic compositions similar to rainwater ($^{87}Sr/^{86}Sr$ = 0.70945–0.70984; Fig. 5; Table 3) and seem to record the expected effects of extensive dilution by local meteoric waters (ultimately rainfall) with relatively non-radiogenic Sr isotopic signatures (e.g. Aubert et al., 2002). From the high degree of overlap of $^{87}Sr/^{86}Sr$ ratios between the samples of group 2 and rainwater, it is believed that the contribution of bedrock weathering to the stream waters draining the northern compartment of the Roxo creek watershed was not very pronounced (see discussion below).

In contrast, the abrupt elevation of the $^{87}Sr/^{86}Sr$ ratios ($^{87}Sr/^{86}Sr$ = 0.71009–0.71269) in the tributaries crossing active and reclaimed sections of the Aljustrel mining area in the southern part of the catchment (AMD-contaminated water drainages of group 1; Fig. 5; Table 3) indicate a strong interaction between these waters and the underlying radiogenic metamorphic rocks of the Variscan Paleozoic basement (VSC sequence). Furthermore, the consistent decrease in the $^{87}Sr/^{86}Sr$ ratios observed in the stream waters sampled at increasing distances to the mining area (group 3; Fig. 5; Table 3) can be attributed to mixing in varying proportions of a non-radiogenic dilute component (rainfall-runoff) and a more radiogenic component derived from silicate weathering (responsible for the Sr isotopic signatures of group 1 waters).

A comparison of the Sr isotopic data obtained during the sampling period also reveals that the $^{87}Sr/^{86}Sr$ ratios measured at each individual sampling point remain fairly constant in the tributaries from the northern slope (group 2; Fig. 5), but show considerable scatter in the stream waters from the southern compartment (groups 1 and 3; Fig. 5). The uniformity of Sr isotopic compositions displayed by the northern streams points to the dominance of a single and homogeneous Sr source, whereas the temporal fluctuations in the isotopic signal of the southern streams may have been caused by variable inputs of waters derived from different Sr reservoirs.

6. Discussion

6.1. Natural and anthropogenic Sr sources

Natural sources of Sr to surface waters include bedrock, soil solid particles and atmospheric inputs (rainfall and air dust particles) (e.g. Bestland et al., 2017). In order to investigate the potential end-members or contributive areas to the Sr budget of the analysed waters, it is

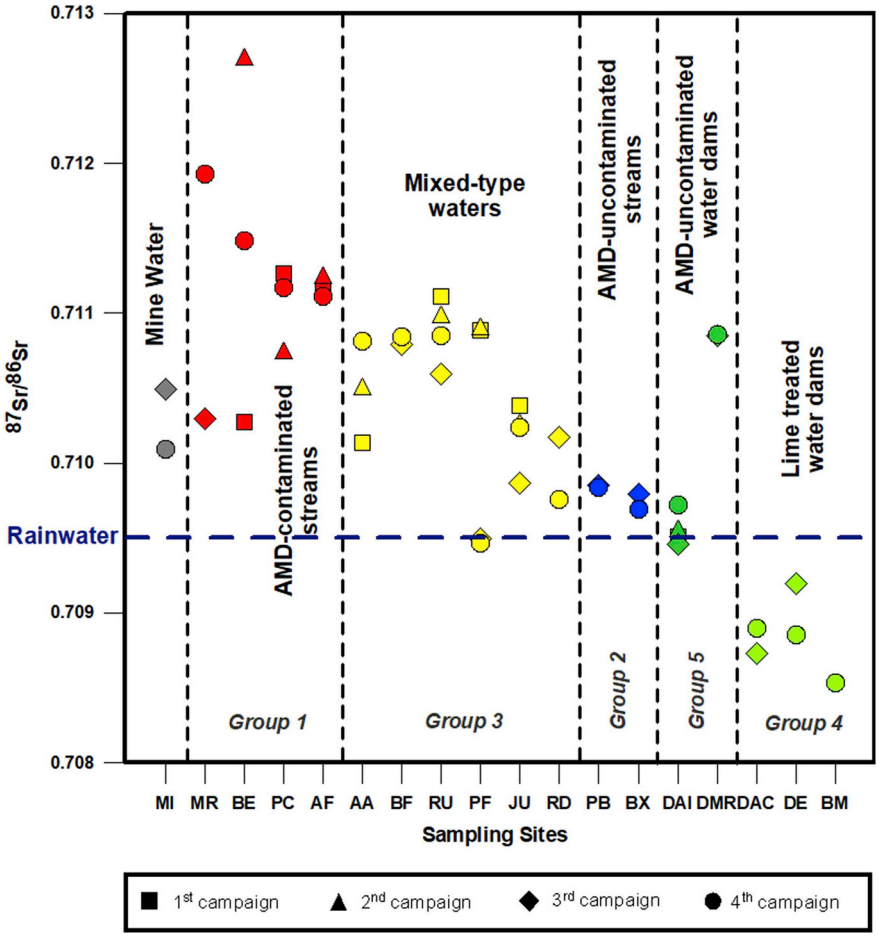

Fig. 5. $^{87}Sr/^{86}Sr$ isotopic ratios for the surface waters from the Roxo Creek watershed. Different symbols stand for the $^{87}Sr/^{86}Sr$ ratios measured in waters from the same sampling site during the four sampling campaigns.

Table 3
Sr isotopic compositions of rainwater and surficial water samples from the Aljustrel region.

Sample ID	$^{87}Sr/^{86}Sr$			
	1st Sampling campaign	2nd Sampling campaign	3rd Sampling campaign	4th Sampling campaign
MI	–	–	0.710494 ± 37	0.710094 ± 33
MR	–	–	0.710297 ± 41	0.711926 ± 47
BE	0.710278 ± 38	0.712694 ± 36	–	0.711482 ± 38
PC	0.711262 ± 38	0.710733 ± 45	–	0.711167 ± 33
AF	0.711160 ± 41	0.711239 ± 31	–	0.711110 ± 26
AA	0.710137 ± 40	0.710491 ± 37	–	0.710810 ± 33
BF	–	–	0.710793 ± 36	0.710841 ± 31
RU	0.711116 ± 41	0.710972 ± 38	0.710598 ± 34	0.710852 ± 30
PF	0.710889 ± 40	0.710894 ± 44	0.709492 ± 26	0.709467 ± 30
JU	0.710387 ± 30	0.710249 ± 43	0.709865 ± 30	0.710240 ± 31
RD	–	–	0.710175 ± 26	0.709757 ± 27
PB	–	–	0.709849 ± 31	0.709837 ± 31
BX	–	–	0.709790 ± 28	0.709688 ± 28
DAI	0.709509 ± 45	0.709546 ± 40	0.709458 ± 35	0.709723 ± 31
DMR	–	–	0.710853 ± 31	0.710858 ± 33
DAC	–	–	0.708727 ± 35	0.708896 ± 28
DE	–	–	0.709196 ± 40	0.708853 ± 37
BM	–	–	–	0.708530 ± 28
Rainwater	0.7094597 ± 33			

Table 4
– Range of published whole-rock Sr isotopic data for different rock units of the Paleozoic basement of the Iberian Pyrite Belt (IPB).

Sample location	Sample lithology	$^{87}Sr/^{86}Sr$	Reference
Late Devonian Phyllite–Quartzite Group (PQ)			
San Jorge Mine (Spain)	Shale - PQ Group	0.733901 ± 8 to 0.748205 ± 8	Tornos (2006)
Catalañas (Spain)	Shale - PQ Group	0.732389 ± 8	Tornos (2006)
Ratera (Spain)	Shale - PQ Group	0.763196 ± 8 to 0.774792 ± 8	Tornos (2006)
Famennian to mid-late Visean Volcano Sedimentary Complex (VSC)			
Feitais (Aljustrel, Portugal)	VSC pyroclastic rocks	0.73008 to 0.78431	Priem et al. (1978)
Feitais (Aljustrel, Portugal)	Volcanic-hosted barite-bearing veins	0.708438 ± 13 to 0.709150 ± 47	Inverno et al. (2008)
Feitais (Aljustrel, Portugal)	Carbonate-quartz-barite veins	0.708836 ± 13 to 0.708877 ± 13	Inverno et al. (2008)
Puebla de Gusmán (Spain)	VSC mafic/intermediate volcanics	0.703775 ± 18 to 0.706687 ± 16	Mitjavila et al. (1997)
Puebla de Gusmán (Spain)	VSC acid volcanics	0.708287 ± 18 to 0.713245 ± 16	Mitjavila et al. (1997)
Neves Corvo (Portugal)	VSC mineralized stockwork ores	0.711374 ± 25 to 0.735563 ± 38	Relvas et al. (2001)
San Jorge Mine (Spain)	Lower VSC shale	0.748044 ± 8 to 0.768081 ± 8	Tornos (2006)
Tharsis (Spain)	Lower VSC shale	0.739500 ± 8 to 0.797371 ± 8	Tornos (2006)

crucial to have reliable information on the Sr isotopic composition of the main lithological units cropping out in the area. Unfortunately, there are no published Sr isotopic analyses for the Cenozoic sedimentary deposits of the Aljustrel region and the available whole-rock isotopic data for the metasedimentary and/or meta-volcanic rocks of the Paleozoic basement are scarce and highly variable. A compilation of the existing data is given in Table 4.

At the scale of the Roxo creek watershed, the influence of bedrock geology on the composition of riverine water is clearly evidenced by differences in the chemical and isotopic characteristics of the stream waters draining the northern and southern compartments (Fig. 6).

In the southernmost part of the study area, the high $^{87}Sr/^{86}Sr$ ratios shown by the mining-impacted tributaries from group 1 (Fig. 6) appear to have been largely controlled by chemical weathering of the underlying

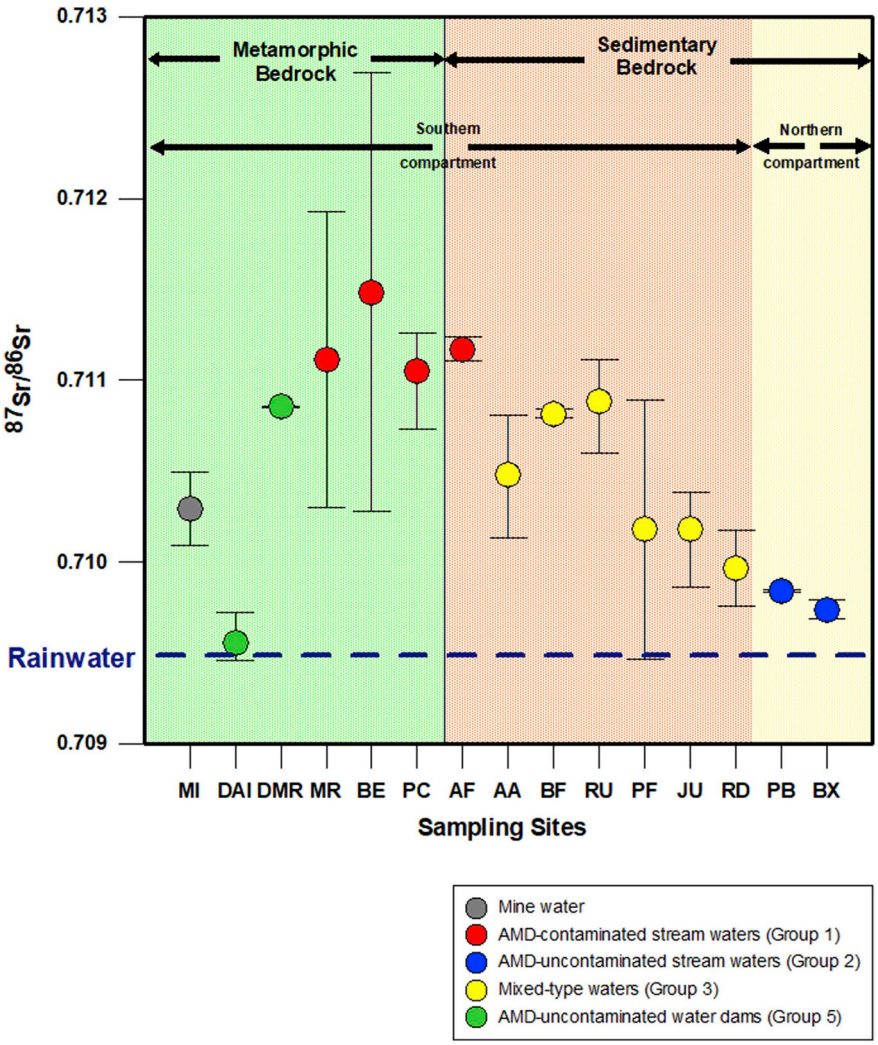

Fig. 6. Sr isotopic variation in the surface waters from the Roxo Creek watershed as a function of bedrock geology. Bars represent the range of observed ratios in surface waters from each individual sampling site and symbols stand for their $^{87}Sr/^{86}Sr$ average ratios.

Paleozoic metamorphic rocks (VSC sequence). The exposed VSC sequence comprises two major felsic volcanic units overlain by massive sulphide ore deposits and capped by a continuous layer of jasper/chert, which grades, towards the top, into purple, green and grey shales (Relvas et al., 2011; Inverno et al., 2015 and references therein). The VSC shales are, in turn, conformably overlain by thick turbidite deposits of the Baixo Alentejo Flysch Group (Relvas et al., 2011 and references therein).

Due to the considerable lithological diversity of the Paleozoic basement, the various source materials contributing to the waters of group 1 are not easily identified. However, it is worth noting that the measured $^{87}Sr/^{86}Sr$ ratios for this group of water samples ($^{87}Sr/^{86}Sr$ = 0.71009–0.71269) are significantly lower than those of the VSC metapelites ($^{87}Sr/^{86}Sr$ = 0.73950 to 0.79737; Table 4) and lie within the interval of values reported for the mineralized acid volcanic rocks of the VSC ($^{87}Sr/^{86}Sr$ = 0.70828–0.71324; Table 4), suggesting that the acid volcanic units and associated mineralizations constitute the main reactive weathering end-member for this portion of the watershed.

The acid volcanic rocks from the VSC range from dacites to high-silica rhyolites and are composed by porphyritic quartz and feldspar (Na-plagioclase and minor K-feldspar) set in a highly altered sericite-chlorite-carbonate groundmass, whilst the neighboring metapelites consist essentially of phyllosilicates and minor amounts of quartz (Mitjavila et al., 1997; Rosa et al., 2010; Relvas et al., 2011). Under extremely acid conditions (pH < 4) caused by the oxidation of pyrite from the mineralized veins and enhanced through mining and milling processes, it is likely that the dissolution of the aluminosilicates (mainly Na-plagioclase) from the adjacent dacites and rhyolites was greatly promoted (e.g. Blum et al., 1993; Probst et al., 2000; Capo et al., 2001).

Thus, silicate weathering is thought to have been the major factor controlling the highly radiogenic signatures and the elevated Al concentrations observed in the waters of group 1, while the concomitant oxidation of metal sulphide minerals (e.g. pyrite) can account for their high dissolved sulphate and heavy metal/metalloid contents. Furthermore, the large scatter of $^{87}Sr/^{86}Sr$ ratios observed in this group of samples is probably related to the lithological heterogeneity of the metamorphic bedrock.

Down-gradient of the mining area, the tributaries of the Roxo creek become progressively more depleted in SO_4, heavy metals/metalloids and radiogenic Sr (group 3; Fig. 6), whereas the waters flowing through the Cenozoic rocks from the northern compartment have Sr isotopic compositions similar to rainwater and negligible concentrations of SO_4 and heavy metals/metalloids (group 2; Fig. 6). The variation pattern recorded in these two groups of stream waters is consistent with a decreasing influence of water-rock interaction processes and an increasing contribution of a non-radiogenic dilute component (rainfall/runoff) with increasing distance to the mining area.

As the Cenozoic deposits of the Sado Basin were most probably derived from erosion of the Paleozoic basement, it can be presumed that their Sr isotope signatures are not significantly different from those of their parent rocks. Nevertheless, the continuous decline of $^{87}Sr/^{86}Sr$ ratios displayed by the water samples from groups 2 and 3 reveals that the input of radiogenic Sr leached from primary silicates and/or clay components of the clastic bedrock was small. This may result from the higher abundances of low reactivity mineral phases (quartz + K-feldspar + micas + clay minerals) relative to plagioclase in these sediments (e.g. Bullen et al., 1996; Probst et al., 2000; Frost and Toner, 2004; Blum and Erel, 2005). In addition to mineralogical composition, the poorly lithified nature of the siliciclastic units from the Sado Basin and the short residence time of percolating meteoric water are other parameters that could have contributed to enhance the atmospheric signal (rainfall/runoff) in the Sr isotope budget of these stream waters and to explain the lower silicate denudation rates prevailing in the northern sector.

Although weathering and ion exchange reactions with silicate minerals from the Cenozoic deposits appear to have had little effect on the Sr isotope compositions of the surface waters from groups 2 and 3, the concentrations of Na and Cl in the stream waters from the northern compartment (group 2) and some tributaries from group 3 (Fig. 3) are well in excess of Aljustrel precipitation pointing to the involvement of an additional source for Na and Cl. Such a source could have been provided by the local occurrence of finely disseminated evaporite layers within the Cenozoic stratigraphic sequence, as already mentioned by Schermerhorn et al. (1987). Owing to their high soluble characteristics and relatively unradiogenic Sr isotope signatures, the dissolution of halite bearing deposits may have been responsible for the increase of Cl and Na contents in the dissolved load of these waters (e.g. Millot et al., 2003) with no detectable influence on their Sr isotope ratios (close to local rainwater). Moreover, the high levels of Sr observed in these samples suggests that the source of Cl is also a potential source of Sr (e.g. Kloppmann et al., 2001; Négrel et al., 2007; Zieliński et al., 2016).

A fourth end-member of anthropogenic origin must also be considered to explain the low Sr isotope ratios found in the samples collected in the lime-treated water dams (DAC, DE) and one tributary fed by the DE dam (BM) (Fig. 5). The use of Sr-rich lime (CaO) or $CaCO_3$ for mitigation of environmental impacts associated with AMD can lead to a marked decrease of $^{87}Sr/^{86}Sr$ ratios in the pond waters (Christian et al., 2011; Khaska et al., 2015; Harkness et al., 2016), being the most likely cause for the anomalously low Sr isotope ratios and high Sr and Ca contents displayed by these water samples.

In summary, we interpret most of the spatial variability of Sr isotope compositions in the analysed water samples in terms of mixing of waters derived from several source reservoirs. The most radiogenic end-member is represented by the stream waters draining the mineralized Variscan Paleozoic formations from the southern compartment and corresponds to a silicate weathering component, enhanced by mining activities that promote AMD processes. By contrast, the low $^{87}Sr/^{86}Sr$ signatures of the tributaries from the northern section reveal a dominant contribution of a non-radiogenic meteoric end-member (rainfall/runoff). This meteoric input is related to the low weathering rates of the Cenozoic siliciclastic rocks exposed in the northern part of the catchment, highlighting the role played by geological setting on the Sr isotope budget of riverine waters. Dissolution of disseminated halite does not seem to influence to a significant degree the Sr isotope ratios of these tributaries, but has probably contributed to elevate their Sr concentrations (Kloppmann et al., 2001; Négrel et al., 2007; Zieliński et al., 2016). Finally, evidence of an anthropogenic source with very low $^{87}Sr/^{86}Sr$ ratios is provided by the samples from the two lime-treated water dams and BM stream waters.

6.2. Mixing relationships

The $^{87}Sr/^{86}Sr$ ratio *vs.* 1/Sr diagram is classically used to evaluate two-component mixing and end-member water compositions (e.g. Négrel et al., 2001, 2007). Water samples derived from mixing of two sources typically produce linear trends on the $^{87}Sr/^{86}Sr$ ratio *vs.* 1/Sr diagram, but will tend to scatter in several directions if more than two sources are involved (e.g. Négrel et al., 2007; Bestland et al., 2017). End-member uncertainty is frequently a major issue and may prevent a direct quantification of mixing relationships, particularly in the cases where multiple sources are involved, such as the present one. Nonetheless, the observed trends can provide some constraints on both the nature of source reservoirs and the extent of water-rock interaction processes.

As shown in Fig. 7, the analysed water samples do not define a single mixing line on the $^{87}Sr/^{86}Sr$ ratio *vs.* 1/Sr diagram. However, most of the AMD-contaminated waters from the southern compartment seem to plot along a linear array (path “a”, Fig. 7) between a non-radiogenic source reservoir represented by local rainwater with $^{87}Sr/^{86}Sr$ ratios ≈0.7095 and high 1/Sr ratios (stored at the DAI waterproofing dam) and a more radiogenic end-member corresponding to the Sr released from the weathered Variscan metamorphic formations ($^{87}Sr/^{86}Sr$ > 0.7100; 1/Sr < 6).

The mine discharge waters collected at site MI are the only samples that do not fall in the main trend. Their shift towards very low 1/Sr

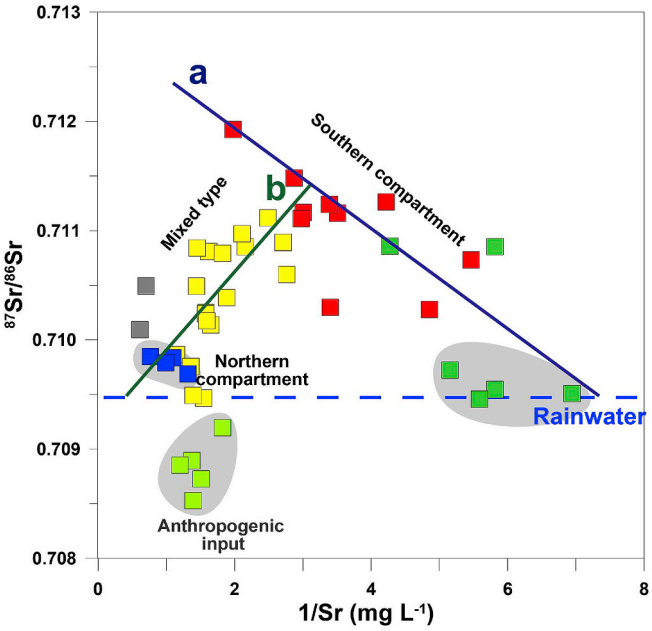

Fig. 7. $^{87}Sr/^{86}Sr$ *vs.* 1/Sr diagram for the surface waters from the Aljustrel region. Symbols as before (Fig. 3).

ratios presumably reflects a complex and deep-seated origin, involving the contribution of released Sr from gangue carbonates and/or introduction of Sr from anthropogenic sources brought with groundwater into the mine (Heidel et al., 2007). Inverno et al. (2008) report the occurrence of carbonate-quartz-barite veins cutting the Aljustrel orebody with $^{87}Sr/^{86}Sr$ ratios ranging between 0.708836 and 0.708877 (Table 4). The local dissolution of such carbonates could have been responsible for the elevation of Sr and Ca contents in MI waters (Fig. 3) and the decrease of their $^{87}Sr/^{86}Sr$ ratios.

Compared to the AMD-contaminated waters, the samples from the tributaries draining the northern compartment are tightly clustered around $^{87}Sr/^{86}Sr$ values ranging between 0.7095 and 0.7098 and 1/Sr ratios less than 2 (Fig. 7), indicating a large homogeneity of the water source for this sector of the watershed. Although the similarity of their Sr isotopic signatures with those of local rainwater points to dominant atmospheric input to these stream waters, their relative enrichment in Sr, Na and Cl suggests that the percolating meteoric waters gained these elements from near-surface weathering and wash-out of Cenozoic deposits containing finely disseminated halite layers.

Down-gradient of the Aljustrel mining area, the tributaries from the southern compartment flow across terranes of contrasted lithologies (Paleozoic basement and Cenozoic deposits) and define a mixing trend between the low-$^{87}Sr/^{86}Sr$ atmospheric end-member and the high-$^{87}Sr/^{86}Sr$ silicate end-member (path "b", Fig. 7), providing compelling evidence for the mixed influence of meteoric inputs and water–rock interactions in these water samples.

The anthropogenic impact caused by the addition of Sr-rich lime is well documented by the low $^{87}Sr/^{86}Sr$ ratios and high Sr contents observed in the samples from the DAC and DE water dams and BE effluent (Fig. 7), but does not seem have significantly affected the compositions of the remaining water samples.

7. Conclusions

The main conclusions of this study are summarized as follows:

1. The Roxo Creek watershed is located in a geologically complex area of South Portugal and can be subdivided into two compartments: (a) the southern compartment is underlain by metamorphic rocks of the Variscan Paleozoic basement hosting massive sulphide ore deposits (Aljustrel mining area) and by Cenozoic sedimentary rocks from the Sado Basin, (b) the northern compartment is dominated by the siliciclastic formations of the Sado Basin and does not bear any mining activity.
2. Geochemical and Sr isotope analyses of surface waters draining the two compartments reveal that the southern tributaries correspond to AMD-contaminated waters showing pH < 4, high dissolved heavy metal/metalloid contents and $^{87}Sr/^{86}Sr$ ratios ranging from 0.7101 to 0.7126, while the northern tributaries are uncontaminated waters with pH > 8, relatively high Cl and Na concentrations and Sr isotopic compositions similar to rainwater ($^{87}Sr/^{86}Sr$ = 0.7097–0.7098). Evidence for an anthropogenic input caused by lime addition is provided by the elevated Ca, Mg and Sr contents and unradiogenic Sr isotope signatures ($^{87}Sr/^{86}Sr$ = 0.7085–0.7091) observed in samples collected at two lime-treated water dams from the mining area.
3. Variations in the $^{87}Sr/^{86}Sr$ ratios and Sr concentrations of the analysed waters are attributed to mixing of two main end-members: meteoric waters (local rainfall/runoff) with low Sr contents and $^{87}Sr/^{86}Sr$ ratios ≈ 0.7095 and more radiogenic waters derived from the Aljustrel mining area. The highly radiogenic signatures of the southern tributaries appear to have been controlled by weathering of plagioclase from the acid volcanic rocks of the Paleozoic basement, enhanced by the high acidity generated by mining activities (pyrite oxidation), although released strontium from gangue carbonates could have locally contributed to the fluctuations of Sr contents and $^{87}Sr/^{86}Sr$ ratios observed in some of these water samples. By contrast, the low $^{87}Sr/^{86}Sr$ ratios and relatively high Sr (Cl and Na) concentrations shown by the surface waters draining the northern compartment suggest that these tributaries correspond to meteoric waters that have gained Cl, Na and Sr through wash-out of Cenozoic deposits containing finely disseminated halite layers. Finally, the decrease in the $^{87}Sr/^{86}Sr$ ratios and elevation of Sr contents observed in the samples from the lime-treated water dams support the involvement of an anthropogenic source of Sr with $^{87}Sr/^{86}Sr$ ratios lower than that of rainfall.

Acknowledgements

This research was supported by GeoBioTec – Department of Geosciences, University of Aveiro, Portugal through FCT/MEC (Project FCT UID/GEO/04035/2013) and by Fundação para a Ciência e a Tecnologia, Portugal (grant numbers SFRH/BPD/99448/2014 and SFRH/BPD/81059/2011).

Appendix A. Supplementary data

Supplementary data to this article can be found online at https://doi.org/10.1016/j.apgeochem.2019.01.016.

References

Åberg, G., 1995. The use of natural strontium isotopes as tracers in environmental studies. Water, Air, Soil Pollut. 79, 309–322.

Åberg, G., Jacks, G., Hamilton, P.J., 1989. Weathering rates and $^{87}Sr/^{86}Sr$ ratios: an isotopic approach. J. Hydrol 109, 65–78.

Aubert, D., Probst, A., Stille, P., Viville, D., 2002. Evidence of hydrological control of Sr behavior in stream water (Strengbach catchment, Vosges mountains, France). Appl. Geochem. 17, 285–300. https://doi.org/10.1016/S0883-2927(01)00080-4.

Barriga, F.J.A.S., 1990. Metallogenesis in the Iberian pyrite Belt. In: Dallmeyer, R.D., y Martínez-García, E. (Eds.), Pre-Mesozoic Geology of Iberia. Springer-Verlag, Berlin, Heidelberg, New York, pp. 369–379.

Barriga, F.J.A.S., Carvalho, D., 1983. Carboniferous volcanogenic sulphide mineralizations in south Portugal (Iberian Pyrite Belt). In: Lemos de Sousa, J.M., Oliveira, J.T. (Eds.), The Carboniferous of Portugal. Memórias dos Serviços Geológicos de Portugal, pp. 99–113.

Barriga, F.J.A.S., Fyfe, W.S., 1998. Multi-phase water-rhyolite interaction and ore fluid generation at Aljustrel, Portugal. Miner. Deposita 33, 188–207. https://doi.org/10.1007/s001260050140.

Bataille, C.P., Bowen, G.J., 2012. Mapping $^{87}Sr/^{86}Sr$ variations in bedrock and water for

large scale provenance studies. Chem. Geol. 304–305, 39–52.
Beard, B.L., Johnson, C.M., 2000. Strontium isotope composition of skeletal material can determine the birth place and geographic mobility of humans and animals. J. Forensic Sci. 45 (5), 1049–1061.
Bentley, R.A., Wahl, J., Price, T.D., Atkinson, T.C., 2008. Isotopic signatures and hereditary traits: snapshot of a Neolithic community in Germany. Antiquity 82 (316), 290–304.
Bestland, E., George, A., Green, G., Olifent, V., Mackay, D., Whallen, M., 2017. Groundwater dependent pools in seasonal and permanent streams in the Clare Valley of South Australia. J. Hydrol: Reg. Stud. 9, 216–235. https://doi.org/10.1016/j.ejrh.2016.12.087.
Blum, J.D., Erel, Y., 2005. Radiogenic isotopes in weathering and hydrology. In: Drever, J.I. (Ed.), Surface and Ground Water, Weathering, and Soils. Treatise on Geochemistry. Elsevier, pp. 365–392.
Blum, J.D., Erel, Y., Brown, K., 1993. $^{87}Sr/^{86}Sr$ ratios of Sierra Nevada stream waters: implications for relative mineral weathering rates. Geochem. Cosmochim. Acta 57, 5019–5025. https://doi.org/10.1016/S0016-7037(05)80014-6.
Böhlke, J.K., Horan, M., 2000. Strontium isotope geochemistry of groundwaters and streams affected by agriculture, Locust Grove, MD. Appl. Geochem. 15, 599–609. https://doi.org/10.1016/S0883-2927(99)00075-X.
Brennan, S.R., Fernandez, D.P., Mackey, G., Cerling, T.E., Bataille, C.P., Bowen, G.J., Wooller, M.J., 2014. Strontium isotope variation and carbonate versus silicate weathering in rivers from across Alaska: implications for provenance studies. Chem. Geol. 389, 167–181. https://doi.org/10.1016/j.chemgeo.2014.08.018.
Brenot, A., Baran, N., Petelet-Giraud, E., Négrel, P., 2008. Interaction between different water bodies in a small catchment in the Paris basin (Brévilles, France): tracing of multiple Sr sources through Sr isotopes coupled with Mg/Sr and Ca/Sr ratios. Appl. Geochem. 23, 58–75. https://doi.org/10.1016/j.apgeochem.2007.09.006.
Bullen, T.D., Krabbenhoft, D.P., Kendall, C., 1996. Kinetic and mineralogic controls on the evolution of groundwater chemistry and $^{87}Sr/^{86}Sr$ in a sandy silicate aquifer, northern Wisconsin, USA. Geochem. Cosmochim. Acta 60, 1807–1821.
Candeias, C., Ferreira da Silva, E., Salgueiro, A.R., Pereira, H.G., Reis, A.P., Patinha, C., Matos, J.X., Ávila, P.H., 2011. Assessment of soil contamination by potential toxic elements in the Aljustrel mining area in order to implement soil reclamation strategies. Land Degrad. Dev. 22, 565–585.
Capo, R.C., Stewart, B.W., Chadwick, O.A., 1998. Strontium isotopes as tracers of ecosystem processes: theory and methods. Geoderma 82, 197–225. https://doi.org/10.1016/S0016-7061(97)00102-X. (pp.21).
Capo, R.C., Winters, W.R., Weaver, T.J., Stafford, S.L., Hedin, R.S., Stewart, B.W., 2001. Hydrogeologic and geochemical evolution of deep mine discharges, Irwin syncline, Pennsylvania. In: Proc 22nd West Virginia Surface Mine Drainage Task Force Symp, pp. 144–153.
Carvalho, D., Barriga, F., Munhá, J., 1999. Bimodal siliciclastic systems: the case of the Iberian pyrite Belt. Rev. Econ. Geol. Soc. Econ. Geol. 8, 375–408. https://doi.org/10.5382/Rev.08.
Carvalho, E., Diamantino, C., Pinto, R., 2016. Environmental remediation of abandoned mines in Portugal - balance of 15 Years of activity and new perspectives. In: Proceedings of the Annual Conference of the International Mine Water Association - IMWA 2016, Mining Meets Water – Conflicts and Solutions, Leipzig, Germany, pp. 554–561.
Chambel, A., Almeida, C., 2000. Geochemical processes affecting the composition of mineral waters in the South Portuguese Zone (Portugal). In: Sililo (Ed.), Groundwater: Past Achievements and Future Challenges, pp. 471–474 © 2000 Balkema, Rotterdam.
Chamberlain, C.P., et al., 1997. The use of isotope tracers for identifying populations of migratory birds. Oecologia 109 (1), 132–141.
Chapman, E.C., Capo, R.C., Stewart, B.W., Hedin, R.S., Weaver, T.J., Edenborn, H.M., 2013. Strontium isotope quantification of siderite, brine and acid mine drainage contributions to abandoned gas well discharges in the Appalachian Plateau. Appl. Geochem. 31, 109–118. https://doi.org/10.1016/j.apgeochem.2012.12.011.
Christian, L.N., Banner, J.L., Mack, L.E., 2011. Sr isotopes as tracers of anthropogenic influences on stream water in the Austin, Texas, area. Chem. Geol. 282, 84–97. https://doi.org/10.1016/j.chemgeo.2011.01.011.
Deng, Y., Wang, Y., Ma, T., 2009. Isotope and minor element geochemistry of high arsenic groundwater from Hangjinhouqi, the Hetao Plain, Inner Mongolia. Appl. Geochem. 24, 587–599.
Faure, G., 1986. Principles of Isotope Geology, second ed. John Wiley, New York.
Faure, G., Mensing, T.M., 2005. Isotopes: Principles and Applications, third ed. John Wiley & Sons, Hoboken (NJ).
Frei, K.M., Frei, R., 2011. The geographic distribution of strontium isotopes in Danish surface waters - a base for provenance studies in archaeology, hydrology and agriculture. Appl. Geochem. 26, 326–340. https://doi.org/10.1016/j.apgeochem.2010.12.006.
Frost, C.D., Toner, R.N., 2004. Strontium isotopic identification of water-rock interaction and ground water mixing. Gr. Water 42, 418–432.
Frost, C.D., Pearson, B.N., Ogle, K.M., Heffern, E.L., Lyman, R.M., 2002. Sr isotope tracing of aquifer interactions in an area of accelerating coal-bed methane production, Powder River Basin, Wyoming. Geology 30, 923–926.
Gaspar, O., 1996. Microscopia e petrologia de minérios, aplicada à génese, exploração e mineralurgia dos sulfuretos maciços dos jazigos de Aljustrel e Neves Corvo. Estud. Notas e Trab 38, 3–195.
Harkness, J.S., Sulkin, B., Vengosh, A., 2016. Evidence for coal ash ponds leaking in the southeastern United States. Environ. Sci. Technol. 50 (12), 6583–6592. https://doi.org/10.1021/acs.est.6b01727.
Heidel, C., Tichomirowa, M., Matschullat, J., 2007. Lead and strontium isotopes as indicators for mixing processes of waters in the former mine "Himmelfahrt Fundgrube", Freiberg (Germany). Isot. Environ. Health Stud. 43 (4), 339–354. https://doi.org/10.1080/10256010701701657.
Hodell, D.A., Quinn, R.L., Brenner, M., Kamenov, G., 2004. Spatial variation of strontium isotopes (Sr-87/Sr-86) in the Maya region: a tool for tracking ancient human migration. J. Archaeol. Sci. 31 (5), 585–601. https://doi.org/10.1016/j.jas.2003.10.009.
Hoppe, K.A., Koch, P.L., Carlson, R.W., Webb, S.D., 1999. Tracking mammoths and mastodons: reconstruction of migratory behavior using strontium isotope ratios. Geology 27 (5), 439–442.
Hosono, T., Nakano, T., Igeta, A., Tayasu, I., Tanaka, T., Yachi, S., 2007. Impact of fertilizer on a small watershed of Lake Biwa: use of sulfur and strontium isotopes in environmental diagnosis. Sci. Total Environ. 384, 342–354. https://doi.org/10.1016/j.scitotenv.2007.05.033.
Hosono, T., Siringan, F., Yamanaka, T., Umezawa, Y., Onodera, S. ichi, Nakano, T., Taniguchi, M., 2010. Application of multi-isotope ratios to study the source and quality of urban groundwater in Metro Manila, Philippines. Appl. Geochem. 25, 900–909. https://doi.org/10.1016/j.apgeochem.2010.03.009.
Inverno, C., Solomon, M., Barton, M.D., Foden, J., 2008. The Cu stockwork and massive sulfide ore of the Feitais volcanic-hosted massive sulfide deposit, Aljustrel, Iberian pyrite introduction and geological setting of the Iberian pyrite Belt. In: Weihed, P. (Ed.), 3D, 4D and Predictive Modelling of Major Mineral Belts in Europe. Mineral Resource Reviews. Springer International Publishing, Switzerland, pp. 191–208. https://doi.org/10.1007/978-3-319-17428-0_9.
Inverno, C., Díez-Montes, A., Rosa, C., García-Crespo, J., Matos, J., García-Lobón, J.L., Carvalho, F., Bellido, F., Castello-Branco, J.M., Ayala, C., Batista, M.J., Rubio, F., Granado, I., Tornos, F., Oliveira, J.T., Rey, C., Araújo, V., Sánchez-García, T., Pereira, Z., Represas, P., Solá, A.R., Sousa, P., 2015. Introduction and geological setting of the Iberian pyrite Belt. In: Weihed, P. (Ed.), 3D, 4D and Predictive Modelling of Major Mineral Belts in Europe. Mineral Resource Reviews. Springer International Publishing, Switzerland, pp. 191–208. https://doi.org/10.1007/978-3-319-17428-0_9.
Jeon, S.R., 2008. Hydrochemical, and Pb- and Sr- isotopic constraints on the precipitation and dilution of metals in acidified mine water: an example from the abandoned Dongjin Au-Ag-Cu mine, Korea. Geosci. J. 12, 411–418. https://doi.org/10.1007/s12303-008-0040-7.
Khaska, M., Le Gal La Salle, C., Verdoux, P., Boutin, R., 2015. Tracking natural and anthropogenic origins of dissolved arsenic during surface and groundwater interaction in a post-closure mining context: isotopic constraints. J. Contam. Hydrol. 177–178, 122–135.
Kelly, S., Heaton, K., Hoogewerff, J., 2005. Tracing the geographical origin of food: the application of multi-element and multi-isotope analysis. Trends Food Sci. Technol. 16 (12), 555–567. https://doi.org/10.1016/j.tifs.2005.08.008.
Kloppmann, W., Négrel, P., Casanova, J., Klinge, H., Schelkes, K., Guerrot, C., 2001. Halite dissolution derived brines in the vicinity of a Permian salt dome (N German Basin). Evidence from boron, strontium, oxygen, and hydrogen isotopes. Geochem. Cosmochim. Acta 65, 4087–4101.
Koch, P.L., et al., 1995. Isotopic tracking of change in diet and habitat use in African elephants. Science 267 (5202), 1340–1343.
Leistel, J.M., Marcoux, E., Thiéblemont, D., Quesada, C., Sánchez, A., Almodóvar, G.R., Pascual, E., Sáez, R., 1998. The volcanic-hosted massive sulphide deposits of the Iberian pyrite Belt review and preface to the thematic issue. Miner. Deposita 33, 2–30. https://doi.org/10.1007/s001260050130.
Luís, A.T., Teixeira, P., Almeida, S.F.P., Ector, L., Matos, J.X., Ferreira da Silva, E.A., 2009. Impact of acid mine drainage (AMD) on water quality, stream sediments and periphytic diatom communities in the surrounding streams of Aljustrel mining area (Portugal). Water, Air, Soil Pollut. 200, 147–167.
Luís, A.T., Durães, N., Almeida, S.F.P., Ferreira da Silva, E.A., 2016. Integrating geochemical (surface waters, stream sediments) and biological (diatoms) approaches to assess AMD environmental impact in a pyritic mining area: Aljustrel (Alentejo, Portugal). J. Environ. Sci. 42, 215–226.
Martin-Izard, A., Arias, D., Arias, M., Gumiel, P., Sanderson, D.J., Castañon, C., Sanchez, J., 2016. Ore deposit types and tectonic evolution of the Iberian Pyrite Belt: from transtensional basins and magmatism transpression and inversion tectonics. Ore Geol. Rev. 79, 254–267. https://doi.org/10.1016/j.oregeorev.2016.05.011.
McNutt, R.H., 2000. Strontium isotopes. In: Cook, P., Herczeg, A.L. (Eds.), Environmental Tracers in Subsurface Hydrology. Kluwer Academic Publishers, Boston (MA), pp. 233–260.
Meybeck, M., 1986. Composition chimique naturelle des ruisseaux non pollués en France. Bull. Soc. Géol. 39, 3–77.
Millot, R., Gaillardet, J., Dupré, B., Allègre, C.J., 2003. Northern latitude chemical weathering rates: clues from the Mackenzie River Basin. Canada. Geochem. Cosmochim. Acta 67 (7), 1305–1329.
Mitjavila, J., Martí, J., Soriano, C., 1997. Magmatic evolution and tectonic setting of the Iberian pyrite Belt volcanism. J. Petrol. 38, 727–755.
Montgomery, J., Evans, J.A., Wildman, G., 2006. ^{87}Sr-^{86}Sr isotope composition of bottled British mineral waters for environmental and forensic purposes. Appl. Geochem. 21, 1626–1634.
Munhá, J., 1990. Metamorphic evolution of the south Portuguese/pulo do lobo Zone. In: Dallmeyer, R.D., Martínez García, E. (Eds.), Pre-mesozoic Evolution of Iberia. Springer Verlag, pp. 363–368.
Négrel, P., Casanova, J., Aranyossy, J.-F., 2001. Strontium isotope systematics used to decipher the origin of groundwaters samples from granitoids: the Vienne Case (France). Chem. Geol. 177, 287–308. https://doi.org/10.1016/S0009-2541(00)00414-9.
Négrel, P., Pauwels, H., 2004. Interaction between different groundwaters in Brittany catchments (France): characterizing multiple sources through strontium- and sulphur

isotope tracing. Water, Air, Soil Pollut. 151, 261–285. https://doi.org/10.1023/B:WATE.0000009912.04798.b7.
Négrel, P., Lemiére, B., Macchard de Grammond, H., Billaud, P., Sengupta, B., 2007. Hydrogeochemical processes, mixing and isotope tracing in hard rock aquifers and surface waters from the Subarnarekha River Basin, (east Singhbhum District, Jharkhand State, India). Hydrogeol. J. 15, 1535–1552. https://doi.org/10.1007/s10040-007-0227-4.
Nocete, F., Alex, E., Nieto, J.M., Sáez, R., Bayona, M.R., 2005. An archaeological approach to regional environmental pollution in the south-western Iberian Peninsula related to Third Millennium B.C. mining and metallurgy. J. Archaeol. Sci. 32, 1566–1576.
Oliveira, J.T., 1990. Stratigraphy and synsedimentary tectonism in the south Portuguese Zone. In: Dallmeyer, R.D., Garcia, E.M. (Eds.), Pre-Mesozoic Geology of Iberia. IGCP-Project 233 (Terranes in the Circum-Atlantic Paleozoic Orogens). Springer-Verlag, Berlin, Heidelberg, pp. 334–347. https://doi.org/10.1007/978-3-642-83980-1_23.
Oliveira, J.T., Rosa, C.J.P., Pereira, Z., Rosa, D.R.N., Matos, J.X., Inverno, C.M.C., Andersen, T., 2013. Geology of the Rosário–Neves Corvo antiform, Iberian Pyrite Belt, Portugal: new insights from physical volcanology, palynostratigraphy and isotope geochronology studies. Miner. Deposita 48, 749–766.
Palmer, M.R., Edmond, J.M., 1992. Controls over the strontium isotope composition of river water. Geochem. Cosmochim. Acta 56, 2099–2111.
Peiffer, L., Taran, Y.A., Lounejeva, E., Solís-Pichardo, G., Rouwet, D., Bernard-Romero, R.A., 2011. Tracing thermal aquifers of El Chichón volcano-hydrothermal system (México) with $^{87}Sr/^{86}Sr$, Ca/Sr and REE. J. Volcanol. Geoth. Res. 205, 55–66. https://doi.org/10.1016/j.jvolgeores.2011.06.004.
Pais, J., Cunha, P.P., Pereira, D., Legoinha, P., Dias, R., Moura, D., Silveira, A.B., Kullberg, J.C., González-Delgado, J.A., 2012. The Paleogene and Neogene of western Iberia (Portugal): a cenozoic record in the european atlantic domain. SpringerBriefs in Earth Sciences. https://doi.org/10.1007/978-3-642-22401-0. 156 pp.
Pierson-Wickmann, A.C., Aquilina, L., Weyer, C., Molénat, J., Lischeid, G., 2009. Acidification processes and soil leaching influenced by agricultural practices revealed by strontium isotopic ratios. Geochem. Cosmochim. Acta 73, 4688–4704. https://doi.org/10.1016/j.gca.2009.05.051.
Pimentel, N.L., 1998. Tectono-sedimentary evolution of the Sado Basin (tertiary, southern Portugal). Actas do II Congresso Nacional de Geologia, Lisboa 84 (1), 145–148.
Priem, H.N.A., Boelrijk, N.A.I.M., Hebeda, E.H., Schermerhorn, L.J.G., Verdurmen, E.A.Th, Verschure, R.H., 1978. Sr isotopic homogenization through whole-rock systems under low-greenschist facies metamorphism in carboniferous pyroclastics at Aljustrel (Southern Portugal). Chem. Geol. 21, 307–314. https://doi.org/10.1016/0009-2541(78)90051-7.
Probst, A., El Gh'mari, A., Aubert, D., Fritz, B., McNutt, R., 2000. Strontium as a tracer of weathering processes in a silicate catchment polluted by acid atmospheric inputs. Strengbach, France. Chem Geol 170, 203–219. https://doi.org/10.1016/S0009-2541(99)00248-X.
Relvas, J.M.R., Tassinari, C.C.G., Munhá, J., Barriga, F.J.A.S., 2001. Multiple sources for ore-forming fluids in the Neves Corvo VHMS deposit of the Iberian Pyrite Belt (Portugal): strontium, neodymium and lead isotope evidence. Miner. Deposita 36, 416–427. https://doi.org/10.1007/s001260100168.
Relvas, J.M.R.S., Barriga, F.J.A.S., Ferreira, A., Noiva, P.C., Pacheco, N., Barriga, G., 2006a. Hydrothermal alteration and mineralization in the Neves-Corvo volcanic-hosted massive sulfide deposit, Portugal. I. Geology, mineralogy, and geochemistry. Econ. Geol. 101, 753–790. https://doi.org/10.2113/gsecongeo.101.4.753.
Relvas, J.M.R.S., Barriga, F.J.A.S., Longstaffe, F.J., 2006b. Hydrothermal alteration and mineralization in the Neves-Corvo volcanic-hosted massive sulfide deposit, Portugal. II. Oxygen, hydrogen, and carbon isotopes. Econ. Geol. 101, 791–804. https://doi.org/10.2113/gsecongeo.101.4.791.
Relvas, J.M.R.S., Barriga, F.J.A.S., Carvalho, J.R.S., Pinto, A.M.M., Matos, J.X., Rosa, C.J.P., Pereira, Z., 2011. Structure, stratigraphy and hydrothermal alteration at the Gavião orebodies, Aljustrel: reconstruction of a dismembered ore-forming system at the Iberian Pyrite Belt and implications for exploration. Proceedings of 11th SGA Biennial Meeting Let's Talk Ore Deposits 772–774.
Rosa, C.J.P., McPhie, J., Relvas, J.M.R.S., 2010. Type of volcanoes hosting the massive sulfide deposits of the Iberian Pyrite Belt. Volcanol. Geotherm. Rec. 194, 107–126. https://doi.org/10.1016/j.jvolgeores.2010.05.005.
Sáez, R., Pascual, E., Toscano, M., Almodóvar, G.R., 1999. The Iberian type of volcano-sedimentary massive sulphide deposits. Miner. Deposita 34, 549–570. https://doi.org/10.1007/s001260050220.
Schermerhorn, L.J.G., 1971. An outline stratigraphy of the Iberian pyrite Belt. Bol. Geol. Min. 82, 239–268.
Schermerhorn, L.J.G., Zbyszewski, G., Veiga Ferreira, O., 1987. Carta Geológica de Portugal na escala de 1/50000. Folha 42-D Aljustrel e Notícia Explicativa. Serviços Geológicos de Portugal, Lisboa.
Semhi, K., Clauer, N., Probst, J.L., 2000. Strontium isotope compositions of river waters as records of lithology-dependent mass transfers: the Garonne river and its tributaries (SW France). Chem. Geol. 168, 173–193. https://doi.org/10.1016/S0009-2541(00)00226-6.
Shand, P., Darbyshire, D.P.F., Love, A.J., Edmunds, W.M., 2009. Sr isotopes in natural waters: applications to source characterisation and water-rock interaction in contrasting landscapes. Appl. Geochem. 24, 574–586. https://doi.org/10.1016/j.apgeochem.2008.12.011.
Shin, W.J., Ryu, J.S., Lee, K.S., Park, Y., 2015. Identification of anthropogenic contaminant sources in urbanized streams using multiple isotopes. Environ Earth Sci 73, 8311–8324. https://doi.org/10.1007/s12665-014-3992-0.
Silva, J.B., Oliveira, J.T., Ribeiro, A., 1990. Structural outline. In: Pre-Mesozoic Geology of Iberia. IGCP-Project 233 (Terranes in the Circum-Atlantic Paleozoic Orogens). Springer-Verlag, Berlin, Heidelberg, pp. 348–362. https://doi.org/10.1007/978-3-642-83980-1_24.
Tichomirowa, M., Heidel, C., Junghans, M., Haubrich, F., Matschullat, J., 2010. Sulfate and strontium water source identification by O, S and Sr isotopes and their temporal changes (1997-2008) in the region of Freiberg, central-eastern Germany. Chem. Geol. 276, 104–118. https://doi.org/10.1016/j.chemgeo.2010.06.004.
Thiéblemont, D., Pascual, E., Stein, G., 1998. Magmatism in the Iberian Pyrite Belt: petrological constrains on a metallogenic model. Miner. Deposita 33, 98–110.
Tornos, F., 2006. Environment of formation and styles of volcanogenic massive sulfides: the Iberian Pyrite Belt. Ore Geol. Rev. 28, 259–307. https://doi.org/10.1016/j.oregeorev.2004.12.005.
Vengosh, A., Lindberg, T.T., Merola, B.R., Ruhl, L., Warner, N.R., White, A., Dwyer, G.S., Di Giulio, 2013. Isotopic imprints of mountaintop mining contaminants. Environ. Sci. Technol. 47 (17), 10041–10048. https://doi.org/10.1021/es4012959.
Voerkelius, S., Lorenz, G.D., Rummel, S., Quetel, C.R., Heiss, G., Baxter, M., Brach-Papa, C., Deters-Itzelsberger, P., Hoelzl, S., Hoogewerff, J., Ponzevera, E., Van Bocxstaele, M., Ueckermann, H., 2010. Strontium isotopic signatures of natural mineral waters, the reference to a simple geological map and its potential for authentication of food. Food Chem. 118, 933–940. https://doi.org/10.1016/j.foodchem.2009.04.125.
Yevenes, M.A., Mannaerts, C.M., 2012. Untangling hydrological pathways and nitrate sources by chemical appraisal in a stream network of a reservoir catchment. Hydrol. Earth Syst. Sci. 16, 787–799.
Zieliński, M., Dopieralska, J., Belka, Z., Walczak, A., Siepak, M., Jakubowicz, M., 2016. Sr isotope tracing of multiple water sources in a complex river system, Noteć River, Central Poland. Sci. Total Environ. 548–549, 307–316. https://doi.org/10.1016/j.scitotenv.2016.01.036.